

Chemical Reactions on a Single Linear Chain Show Cooperativity

Zuo Zhang,^{||} Haisen Zhou,^{||} Zhun Xu, Guangqi Wu, Hua Lu,^{*} and Huan Wang^{*}



Cite This: *JACS Au* 2025, 5, 261–270



Read Online

ACCESS |

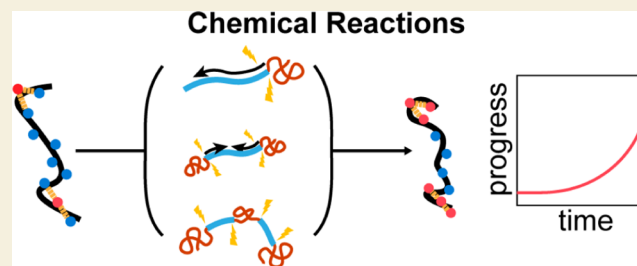
Metrics & More

Article Recommendations

Supporting Information

ABSTRACT: Individual molecules dissolved in a dilute solution are usually considered not to correlate with each other as they undergo chemical reactions due to the mismatch of the diffusion and reaction time scales. Recent studies suggest otherwise, especially for reactions involving macromolecules. With selenopolypeptides as a model system, we used ensemble measurements and single-molecule direct imaging to investigate the correlation between physically constrained chemical reaction sites on a linear polymer chain and the coupling effects between conformation changes and reaction kinetics. We used graphene liquid cells to encapsulate and image the reaction of selenopolypeptides and observed helix-to-coil transitions as Se atoms are oxidized under liquid-phase electron microscopy. Three common pathways were identified among three kinds of selenopolypeptides that differ only in the side groups attached to the Se atoms, which were found to critically determine the observed cooperativity. A more hydrophobic side group appeared to slow the reaction rate, which allowed us to quantify the reaction kinetics in detail and observe the correlation between the reaction sites on a single chain.

KEYWORDS: *single-molecule imaging, helix-to-coil transition, macromolecular reaction, liquid-phase electron microscopy, selenopolypeptide*



INTRODUCTION

Macromolecules differ from small molecules in that their conformations are equilibrated between states upon the thermal fluctuation of solvent molecules. Understanding the interplay between conformational dynamics and reaction kinetics underpins the fundamental chemistry of polymer synthesis. Classical reaction theories explain the kinetics of chemical reactions involving small molecules in diluted solutions. According to the collision theory, reactants collide at an effective collision angle with enough energy and cross the activation energy to form reaction products.¹ According to the theory of transition states, reactants undergo a conformational change along the potential energy surface when they approach each other, which results in the formation of the transition state, followed by reactants crossing the potential barrier to produce products.² Reaction rates are calculated based on the probability of encounter events and exhibit a broad range of reaction orders, such as first-order and second-order kinetics, each shown in distinct reaction curves. Reaction rates are often measured by ensemble methods, assuming that molecules are widely separated and that neighboring reaction events are not mutually influenced. The assumption is reasonable, given the different time scales between bond formation and molecular diffusion. Recent studies observe surprises in reactions involving macromolecules.^{3–7}

For systems involving chemical reactions, cooperativity was discovered during polymerization in polypeptide-based brush macromolecules due to the autocatalysis from macrodipoles

between neighboring α -helices.³ In ring-opening metathesis polymerization (ROMP), from fluorescence-based single-molecule experiments, it was observed that the reaction displayed a range of distinct kinetics, from the first-order to zero-order reaction and single insertion, when the monomer concentration was diluted from 10^{-3} M to 10^{-12} M.⁴ The local chemical environment at the reaction site influences the selectivity of monomer addition, and monomer insertion forms blocks but not a random distribution.⁵ Using tweezer-based single-molecule experiments, the rate of monomer insertion influences the formation of unstable hairball conformations, and the entropic release during conformational interconversion produces forces that mutually influence the reaction rate.⁶ Consequently, molecular diffusion was observed to deviate from the randomization assumption.⁷ On the other hand, neighboring sites have been observed to show cooperative effects in many biochemical reactions, such as protein folding,⁸ enzymatic reactions,⁹ and protein–nucleic acid interaction.¹⁰ The pioneering fluorescence-based single-molecule enzymology experiments showed a correlation between two cholesterol oxidase catalysis turnover events, suggesting that enzymes can

Received: October 3, 2024

Revised: November 29, 2024

Accepted: December 3, 2024

Published: December 16, 2024



catalyze a sequential reaction after forming the active state.¹¹ The cooperativity effects observed in these studies arise from predictable intermolecular interactions. A detailed description of conformational dynamics and reaction kinetics is yet lacking.

To explore the correlation between chemical reaction sites that are physically constrained in space, we consider macromolecular reactions where the reaction takes place at the side chain (Figure 1A). Intermolecular reactions require effective

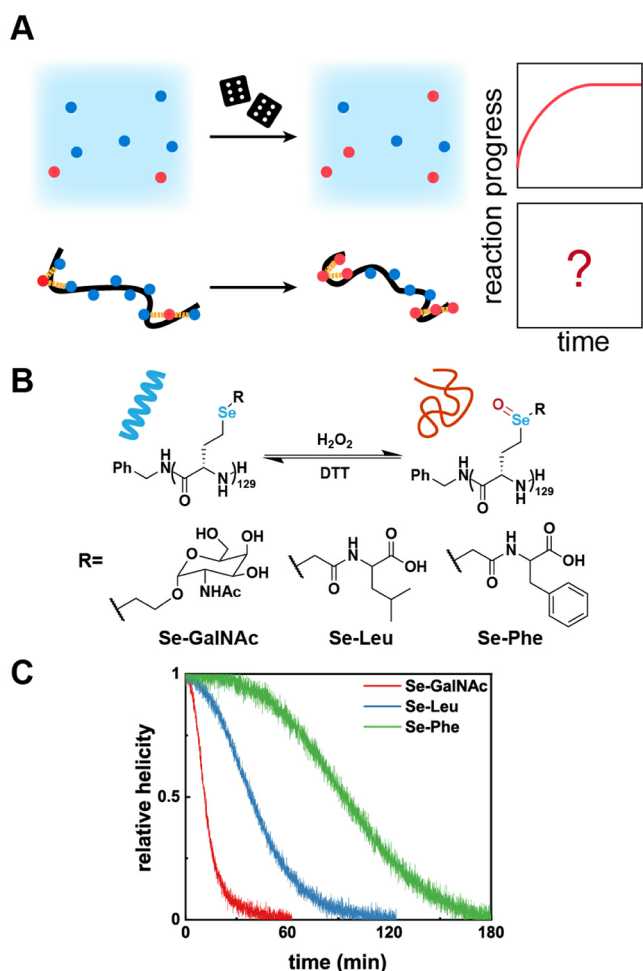


Figure 1. (A) Comparison of chemical reaction kinetics when reaction sites are dispersed in dilute solution or aligned on a single chain. (B) Model system design of selenopolypeptide: polypeptide as the backbone, Se atoms as reaction sites, and different side groups R attached to Se atoms. (C) Relative helicity change was plotted as a function of the reaction time when selenopolypeptides were treated with excess H_2O_2 : 0.5 mg/mL Se-GalNAc in red, 0.25 mg/mL Se-Leu in blue, and 0.25 mg/mL Se-Phe in green, respectively.

collisions between two molecules as they diffuse; such a diffusion may be the rate-limiting process. The intramolecular reaction involves conformational changes and is a better candidate. The helix-coil transition driven by hydrogen bonding among amino acid residues is prevalent in folded proteins; for simplicity and to explore a general mechanism, polypeptides are often used as model molecules to understand reaction dynamics.¹² The transition is usually triggered by heat using laser-induced temperature-jump (T-jump) methods.¹³ Transition dynamics are generally followed by ensemble methods such as circular dichroism spectroscopy (CD),¹⁴ infrared,¹³ fluorescence,¹⁵ Raman,¹⁶ and nuclear magnetic

resonance spectroscopy (NMR).¹⁷ Classical theory describes the helix-to-coil transition as a two-stage process: nucleation and propagation. T-jump study and molecular dynamics simulations both showed disagreement with the theoretical prediction, which led to the development of the conformational diffusion search model.¹⁸ The coil-to-helix process is mainly studied in polypeptide systems, as it simulates the folding of proteins. The phenomena are qualitatively similar when it comes to the helix-to-coil process for polymers, i.e., in the trifluoroacetic acid-induced helix-to-coil transition of poly-norbornene-*g*-poly(γ -benzyl-L-glutamate) (PN-*g*-PBLG).¹⁹ When hydrogen bonds break up entirely, the macromolecule becomes a flexible linear chain, exhibiting a random coil. It is curious to know the role of chain conformation and its adaptation during the reaction and whether it, in turn, impacts the reaction kinetics that occur at each monomer unit along the backbone.

Previous studies mainly rely on ensemble measurements. Fu et al. developed a two-state helix-to-coil transition kinetic theories,²⁰ explaining that cooperativity in brush polymer polymerization reactions arises from intermolecular interactions.²¹ Deming et al. developed functional polymers with a wide range of applications as they undergo helix-coil transition, used as stimuli-controlled microreactors and therapeutic delivery.²² We implemented direct imaging of individual macromolecules to unravel the pathways and kinetics of the reaction occurring on a single chain and resolve their entire backbone conformational adaptation during the reaction. Such experiments are yet lacking, partly because the direct imaging of individual molecules and resolving their backbone conformation in solution require spatial resolution at the nanometer scale and adequate time resolution that could follow the dynamics of interest. This poses a significant challenge, especially when the reaction involves a small molecule: reaction kinetics is too fast to follow, and there is an important trade-off between image resolution and contrast with the imaging frame rate. Ideally, we also want to avoid tags to report the changes of conformation, as the size of tags is usually larger than the monomer unit and may perturb the chain dynamics. The method we used is liquid-phase electron microscopy (LP-EM) with graphene liquid cells, which have been reported to successfully encapsulate synthetic macromolecules,²³ nucleic acids,²⁴ lipids,^{25,26} protein assembly,^{27,28} and enzymes²⁵ and resolve their intermediate states during interaction and assembly.

We selected the synthetic selenopolypeptides, which consist of polyamino acids as the backbone, selenium atoms as the side chain, and the reaction sites to be oxidized to selenoxides in the presence of H_2O_2 , to which the attached groups can be changed to modulate the reactivity (Figure 1B).²⁹ The precise chemical composition is known, and the ensemble reaction kinetics of selenides are well-characterized.^{30–32} The oxidation reaction occurs on the selenium (Se) atoms, and there is precisely one reaction site on each monomer unit with accurate stoichiometry. As the oxidation reaction of the Se atom progresses, the conformation of the polymer changes from a helix to a coil;³⁰ likely due to the shift in hydrophobicity that disrupts the hydrogen bonds between amino acid residues that maintain the helix structure. Such a change in conformation allows us to track the reaction progress in real time by discriminating the shape changes of the molecule using LP-EM without the need for labeling. The presence of the Se atom can also help to increase the image contrast due to its higher

atomic number than the major elements that typically compose the polymer backbone: carbon, oxygen, nitrogen, hydrogen, etc. It is worth noting that selenocysteines are found widely in proteins, and selenium's unique reactivity is used to carry out immunoregulation and antioxidation activities. Studying the oxidation reaction of Se atoms on polypeptide chains can help better understand the underlying mechanisms of such enzymes.³³

RESULTS AND DISCUSSION

Since selenopolypeptides transit from a helix to a coil as Se atoms are oxidized, we performed circular dichroism (CD) experiments to monitor the change of helicity during the helix-to-coil transition to quantify the reaction progress. We synthesized three polymers that differed only in the neighboring groups from the same polymer precursor while keeping the chain length unchanged to evaluate the side group effects on the reaction process. The hydrophilicity of these three groups decreases in the order of GalNac-Leu-Phe (Log *P* from ChemDraw: $-2.13, 0.27, 0.71$, Figure S1). The samples used all have a degree of polymerization of 129, and the molecular masses of Se-GalNac, Se-Leu, and Se-Phe are 53 kDa, 46 kDa, and 51 kDa, respectively. The polydispersity index is 1.13 for all of the polymers, as they are obtained from chemical modification of the same precursor polymer (Figure S2).

We calculated the helicity from the α -helix characteristic peak³⁴ (222 nm) as the oxidation reaction progressed as a function of time in excess H_2O_2 (Figures S3, 1C). The reaction of selenides with H_2O_2 in a dilute solution exhibited second-order (with equivalent H_2O_2) or pseudo-first-order (with excess H_2O_2) reaction kinetics.³¹ Usually, it exhibits an exponential shape obtained from the solution reaction, as shown in Figure 1A.³² However, all three samples showed S-shaped reaction curves from CD measurements, indicating the presence of cooperativity during the reaction progress. Such an effect was not observed in organic selenide monomers distributed separately in solution;³⁵ however, when constrained on a single chain, the cooperativity effect indicated the important coupling between the association of Se atoms with the reaction kinetics. The cooperativity is likely not due to the autocatalysis from the product, which has been ruled out in previous studies of the reaction of aryl selenides with H_2O_2 .³² Alternatively, the difference suggests the arising of cooperative effects as the reaction proceeded, similar to the helix-coil transition triggered by pH changes in the traditional polypeptide system.¹⁹ Ensemble methods such as CD, NMR, and product analysis using mass spectrometry do not probe single-chain kinetics. A single-molecule direct imaging experiment is yet to be implemented, which we report to do with LP-EM to seek answers for reaction pathways and to observe key intermediates.

Evaluation of LP-EM Imaging Conditions

With the sample molecules encapsulated in graphene liquid cells, we used the electron beam to trigger the oxidation reaction and observe the reaction progress in situ and in real time. The radiolytic chemistry of water molecules under an electron beam is well-known: they decompose into several species, including hydrated (solvated) electron e_{h}^- , hydrogen radical $\text{H}\bullet$, hydroxyl radical $\text{OH}\bullet$, H_2 , O_2 , and H_2O_2 . At low electron doses, oxidative species dominate over reducing species and can reach a steady state, maintaining a

concentration of H_2O_2 at 0.1 mM.³⁶ Such a concentration is similar to the reported values for oxidizing selenium peptide into oxidation form in 1 h.²⁹ This justifies why we can use the electron beam to trigger the oxidation reaction of selenium.

The native state of these molecules appears as a slim rod, as they should when maintaining the helix form. For example, the Se-GalNac sample is 22 nm long (Figure S4, Movie S1), consistent with 19.7 nm calculated from a polymerization degree of 129 and 0.55 nm per 3.6 residues.³⁷ The width is about 2.5 nm, which is larger than a typical α -helix diameter. We attribute the deviation to our molecules' much bigger side groups and a relatively loose helical conformation compared to a tight α -helix in proteins. More importantly, the motion-induced blurring in solution has been reported to limit the spatial resolution to 2–3 nm by imaging a double-stranded DNA molecule.²⁴ Motions can include reversible absorptions of the Se-Leu molecule in a graphene liquid cell (Figure S5 and Movie S2), where the molecule diffuses around the absorption sites and jumps between them.

The electron beam creates the oxidizing agent to trigger the reaction, but it could also damage the structure of the polymer. Although it has been used to induce radical polymerization of amphiphilic block copolymers in a liquid environment, and the LP-EM imaging results confirmed the successful formation of the spherical micellar phase from assembly;³⁸ the beam effect can be system-dependent. We evaluated the beam effect and chose imaging conditions carefully.

Under a 200 kV acceleration voltage, we failed to observe the helix-to-coil transition under this condition. Instead, we observed shortening of the slim rod: the total mass and the length of the molecule decreased over time while the average scattering per pixel and the width of the molecule remained stable, indicating an anisotropic degradation of the polymer (Figure S4). The molecule also appeared to be surface-attached, likely due to the formation of hotspots on graphene; as the voltage is higher than its knock-on energy, 80.4 keV, defects can form on graphene. Therefore, the typical experimental conditions we used are 80 keV, $3.0\text{--}6.1 \text{ e}^- \cdot \text{\AA}^{-2} \cdot \text{s}^{-1}$, similar to those used for imaging fragile biomolecules encapsulated in graphene liquid cells,^{25,27,39} We kept a minimal dose and used reducing agents to slow the oxidation reaction, including glycerol and dithiothreitol (DTT), to observe the helix-to-coil transition at its early stage as much as possible. Experimental conditions are listed in Table S1. Despite being in the same graphene liquid pocket, individual molecules do not exhibit similar conformation states even at the beginning of recording the molecular movie. Partly, it could arise from the heterogeneity in the graphene surface, liquid pocket shape, and liquid thickness, which adds to the inherent kinetic heterogeneity of macromolecules. More importantly, pockets form randomly on the graphene sheet. Not all pockets are high-quality pockets containing molecules of interest, so we have to search for target pockets under low magnification, which may have already triggered the reaction before the pocket of interest.²⁵ Given the fast reaction kinetics of Se oxidation, most of the molecules have already been partially or fully oxidized into coils, and the success rate of obtaining an entire pathway is low.

Single-Molecule Reaction Pathways Obtained from LP-EM

TEM images were captured as a continuous series using the in situ mode, and representative images were selected to highlight key intermediates in different pathways. We found three

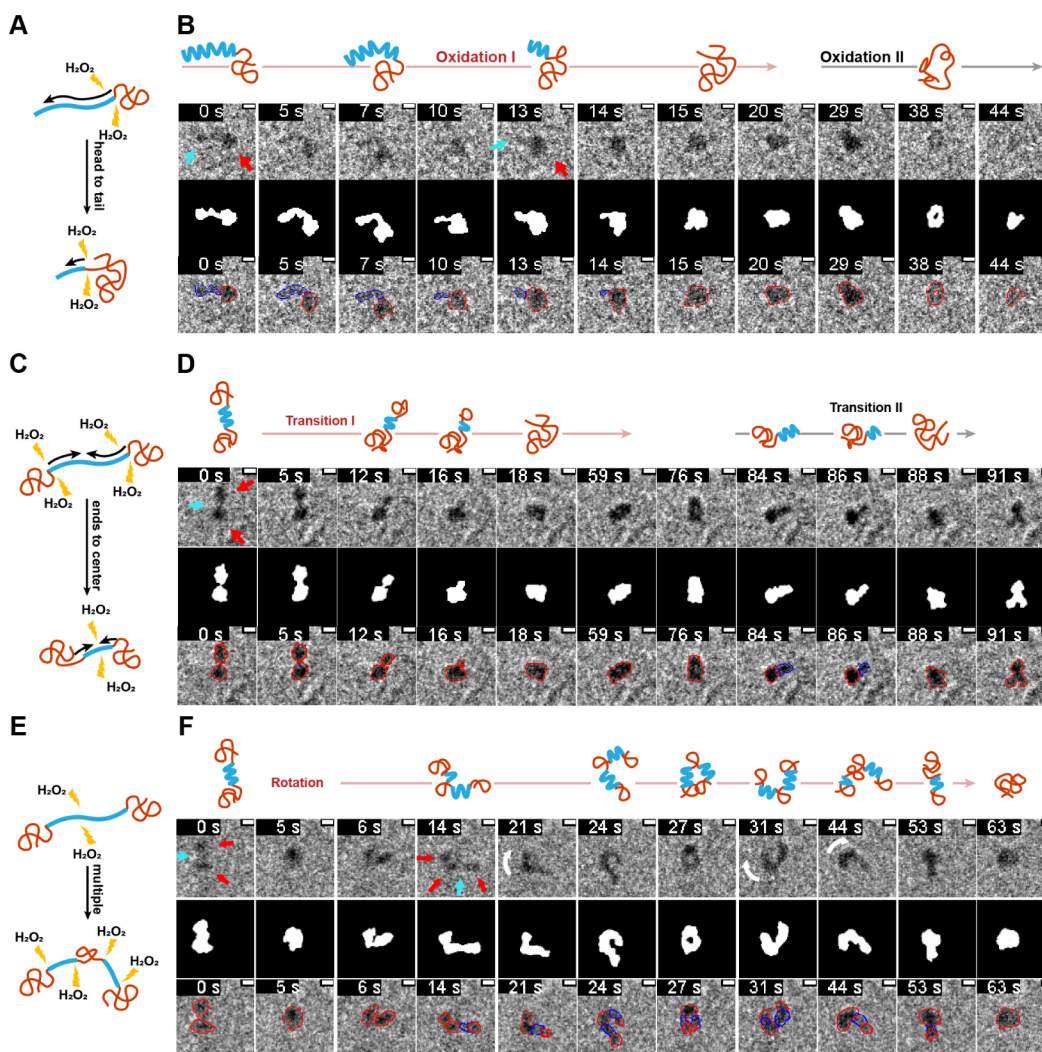


Figure 2. Common pathways observed from the Se-GalNac sample. Schematic (A) and (B) LP-EM images of the “head-to-tail” pathway. Schematic (C,D) LP-EM images of the “ends-to-center” pathway. Schematic (E) and (F) LP-EM images of the “multiple coils” pathway. In (B,D,F), the top panels are the time-lapsed schematic drawings, the second panels are raw data obtained from LP-EM experiments, the third panels are the binarized images corresponding to the raw data, and the bottom panel is the raw data with a blue-colored circle outlining the contour of the helix and a red-colored circle outlining the contour of the coil. Red arrows highlight the coils, cyan arrows highlight the helix, and white arrows highlight the rotation. Scale bar: 5 nm.

pathways of helix-to-coil transition among the three samples, which we describe using data from the Se-GalNac sample. We use the morphological changes from helix (native state) to coil (oxidized state) to indicate the reaction progress. The first reaction pathway is called “head-to-tail” (Figure 2A,B, Movie S3), during which the helix is gradually oxidized into a coil unidirectionally along the polymer backbone. In stage I (0–15 s), Se atoms started to be oxidized, disrupting the hydrogen bonds that hold up the helix. The molecule appeared as a hybrid of a coil head, the oxidized portion, with the unoxidized helix tail (0–15 s). The helix tail is eventually converted to a coil (after 15 s). Quantification confirmed the swallowing of the tail by the head, while the total mass of the molecule remained relatively constant (Figure S6), and the mass per pixel of the head and tail remained stable during the reaction (Figure S7). This analysis suggested that the shape change was due to the helix-to-coil transition rather than the polymer degradation.

The second reaction pathway is called “ends-to-center” (Figure 2C,D, Movie S4), wherein both ends of the polymer

start to react and form coils. The reaction propagates bidirectionally toward the center to eventually form a single large coil: the two balls (coils) at both ends swallow the narrow bridge (helix) connecting them; we attribute it to transition I. Interestingly, following this helix-to-coil transition (0–17 s), we observed the reversible changes of the coil into a helix. The molecule transitioned from a ball to a short rod and maintained it until 82 s; this was followed by another helix-to-coil transition, transition II, which was completed in 6 s (Figure S8). This indicates that even though the oxidation reaction of Se atoms had disrupted the hydrogen bonds among amino acid residues, these hydrogen bonds can reform due to their reversible nature and flexible conformation of a polymer coil. The transition II is not triggered by the oxidation of Se atoms; although it resembles the “head-to-tail” pathway, the underlying driving forces differ.

The third reaction pathway is called “multiple coils” (Figure 2E,F, Movie S5), which involves the formation of an extra coil along the polymer backbone and two coils at the ends. The extra coil usually appears in the central region, generally

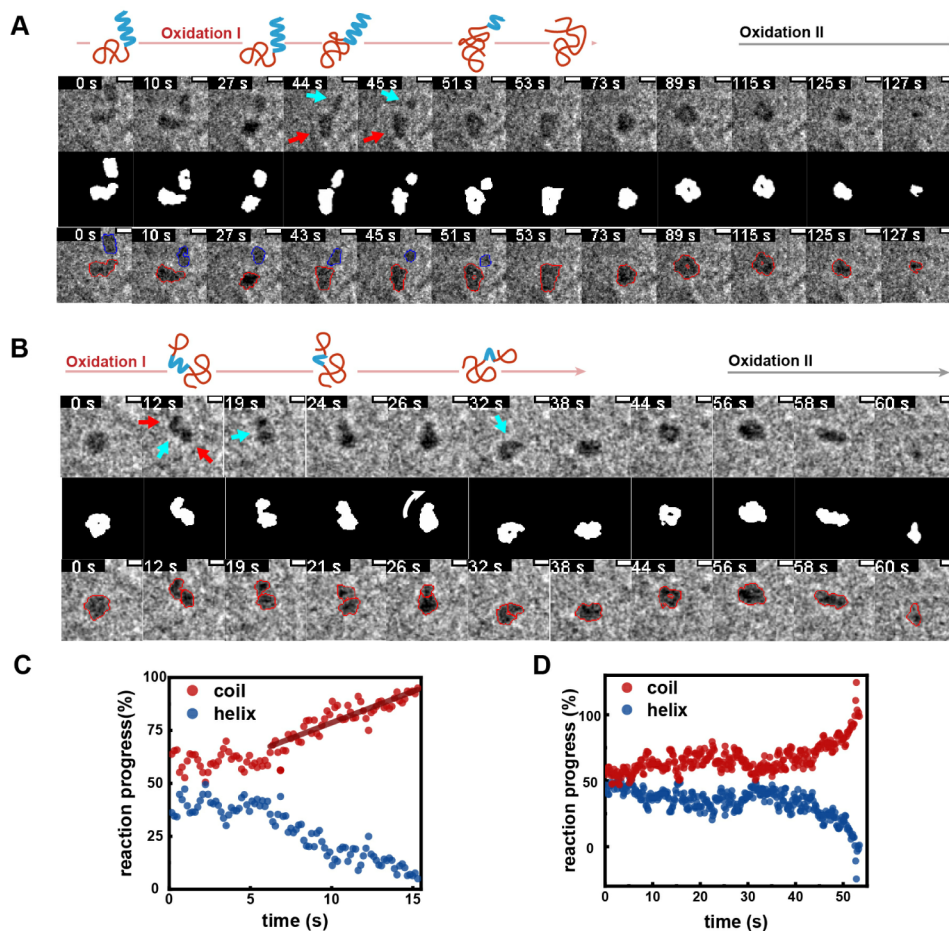


Figure 3. (A) LP-EM images of the “head-to-tail” pathway identified in the Se-Phe sample. Scale bar: 5 nm. (B) LP-EM images of the “ends-to-center” pathway identified in the Se-Leu sample. Scale bar: 5 nm. In (A,B), the top panels are the time-lapsed schematic drawings, the second panels are raw data obtained from LP-EM experiments, the third panels are the binarized images corresponding to the raw data, and the bottom panel is the raw data with a blue-colored circle outlining the contour of the helix and a red-colored circle outlining the contour of the coil. Red arrows highlight the coils, cyan arrows highlight the helix, and white arrows highlight the rotation. Scale bar: 5 nm. (C) The reaction progress of the “head-to-tail” pathway identified from the Se-GalNAC sample corresponds to the LP-EM image series in Figure 2B. The red line shows the linear fit from 6.2 to 15.3 s. (D) The reaction progress of the “head-to-tail” pathway identified from the Se-Phe sample corresponds to the LP-EM image series in (A). The reaction rate increased from 31 to 53 s.

accompanied by drastic rotations of the entire molecule. It is possible that some of the free energy released by the oxidation reaction was transformed into mechanical energy to agitate molecules to rotate. Such rotation allowed more Se atoms embedded inside the narrow bridge (the helix) to be exposed and oxidized with those at the ends.

“Head-to-tail” and “ends-to-center” are also the main pathways identified from data obtained from Se-Phe and Se-Leu samples (Figure 3A,B, and Movies S6 and S7), albeit with slight differences in detailed intermediate conformations. For example, in the Se-Leu sample, the molecule first appeared as a ring (0 s), and at 12 s, it transformed into two smaller coil balls, which then followed the same pathway to produce a larger coil.

Reaction Kinetics and Side Group Influence

Side chain reaction kinetics can be quantified by the percentage of the coil and helix that make up the total mass of the molecule from time-lapsed LP-EM images with image segmentation and analysis methods.⁴⁰ The reaction progress is defined as the ratio of the helix part (marked as blue in TEM images) and coil part (marked as red in TEM images) versus the total mass of the molecule (sum of blue and red parts)

calculated from the gray value in the TEM images. For the “head-to-tail” pathway, the reaction started at 6 s and ended at 15 s, during which we observed a linear dependence of the reaction rate on time for the Se-GalNAC sample (Figure 3C), suggesting the reaction is of zero order. The reaction rate is $2.9\% \text{ s}^{-1}$ from a linear fit. In contrast to the CD results showing an S-shaped curve indicating the cooperativity between adjacent reaction sites, the constant reaction rate obtained from the single-molecule imaging indicates an undetectable correlation. In contrast, the quantitative analysis of the Se-Phe molecules taking the same pathway revealed an increase in the helix–coil conversion rate (Figure 3D). At 30 s, the tail began to fuse into the head, and the process ceased at 53 s. The average reaction rate is $1.8\% \text{ s}^{-1}$, slower than the Se-GalNAC. Strikingly, the reaction progress plot of Se-Phe is nonlinear and shows an increasing trend as the reaction progresses, starting at 40 s. Such an increase indicates the presence of a cooperative effect between neighboring Se atoms residing on a single chain. The cooperativity effect is consistent with the S shape observed from CD experiments.

Both LP-EM experiments and CD measurements report the reaction process from the percentage of the helix. To cross-

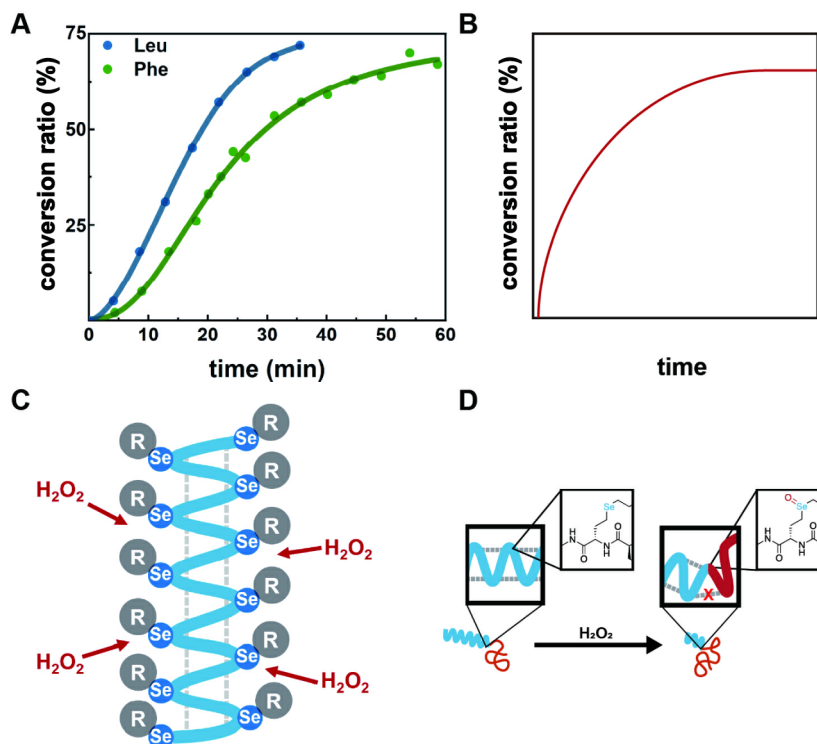


Figure 4. (A) Reaction progress of Se atoms on the peptide backbone when the side group is Phe (Se-Phe) and Leu (Se-Leu70) monitored by NMR (Figures S9–11). (B) Shown for comparison: a representative curve of selenide oxidation by 3 eq H₂O₂ in diluted solutions, as reported in the previous study.³² Reproduced with permission from ref.³² Copyright 2017, John Wiley and Sons. (C) A simple model of selenopolypeptide molecules. (D) Schematic depiction of the side group effect.

validate this, we performed nuclear magnetic resonance (NMR) spectroscopy to report the reaction process by measuring the chemical shift of protons adjacent to the Se atoms. Consistent with these CD results, we observed an S-shaped reaction curve, when the side group is Phe (Se-Phe) and Leu (Se-Leu70, degree of polymerization = 70) (Figures 4A,B and S9–S11). Se-Phe shows more prominent cooperativity, as one can identify from the shape of the curve, and this explains why we observe cooperativity only in Se-Phe from single-molecule imaging experiments.

We also noticed consistency between the average reaction rate obtained from CD measurements and the single-molecule LP-EM experiments. Se-GalNac was oxidized faster than Se-Phe, showing 1.7%·min⁻¹ versus 0.56%·min⁻¹ from the CD results, and 2.9%·s⁻¹ versus 1.8%·s⁻¹ from the LP-EM experiments.

DISCUSSION

Why does the reaction not have an equal probability of occurring on all of the Se atoms on the backbone? In other words, why does a helix not expand to a coil in an isotropic manner? Zimm–Bragg models were proposed 60 years ago and describe the cooperativity in the coil-to-helix transition for polypeptides.^{41,42} The model explains that when the coil-to-helix process is triggered by heating or the solvent composition change, helix propagation is energetically more favorable than nucleation such that the coil ultimately converts into an all-helical conformation. When the degree of polymerization is high, the helical region can appear separately from the coil region, as confirmed by experiments.⁴³ This model describes such a transition arising from molecular interaction. In our study, we observed a similar phenomenon in the coil

expanding in an anisotropic manner, which was shown to be coupled to chemical reactions as the helix travels to the coil.

Despite the difference in the driving force and directionality, we adapted nucleation and elongation ideas in Zimm–Bragg’s theory to rationalize the pathways we observed. Note that, as the helix transits to the coil, the disordered region is produced rather than forming an ordered region designated as nucleation for the coil-to-helix process. We designated the coil region as C and the helix region as H. Unlike natural peptides and nucleic acids, the difference is that Se atom reactions cause the helix-to-coil transition in our system. The reaction likely starts from one end of the polymer, as it has more freedom. Further reaction to a partially reacted molecule CHHHHHH can lead to two scenarios: an expansion of the original coil region to CCHHHHHH or a new coil region CHHHHHHC isolated from the original coil position. The former explains the “head-to-tail” pathway, and the latter describes the “ends-to-center” pathway. Likewise, further reaction to the polymer that undergoes the “ends-to-center” pathway can iterate the above two scenarios, forming a new path when the coil appears at a different position, CHHCHHC, exhibiting the “multiple coils” pathway. The fact that we observed all three pathways confirmed that it is more difficult to react and form a new coil region than to react with Se atoms near existing coil regions. This also reassures us that we can use the secondary structure change, the helix-to-coil transition, to indicate the reaction’s progress. We also acknowledge that this is not sensitive enough to capture the reaction at the very initial stage, where the conformation change is below the spatial resolution, as shown in Figure 3C,D. The location of the new coil can be subject to some randomness from the interchangeable polymer chain conformation, adding extra

complexity to categorize these pathways and quantify the reaction kinetics of the “ends-to-center” pathway and “multiple coils” pathway, especially when the chain length is not too long and spatial resolution also contributes to the uncertainty. Interpretation of some transient states can be subject to some ambiguity. We also want to note that we report the kinetics for the molecules observed to undergo a helix-to-coil transition. We do not rule out the possibilities of other pathways for molecules that already exhibit coil conformation from the beginning of data acquisition.

Why does the reaction prefer to occur near existing coil regions rather than in a new position on the helix? Why do different groups attaching to Se atoms contribute to the overall reaction kinetics and affect the helix-to-coil transition? Selenopolypeptide molecules form a helical structure due to the backbone's hydrogen bonding, similar to the α -helix in amino acids. The reaction sites (Se atoms) are connected to the backbone through two carbon atoms and are somewhat embedded. The side groups GalNAc, Leu, and Phe residues are larger than Se atoms and block the outer layer of the molecule, forming the mask layer between the polymer and the solvent (Figure 4C). Therefore, their hydrophilicity affects the diffusion and effective concentration of H_2O_2 at the interface, which decreases in the order of hydrophilicity: GalNAc > Leu > Phe. The reaction rates measured from CD follow the same trend, decreasing from $1.7\% \cdot \text{min}^{-1}$ to $0.83\% \cdot \text{min}^{-1}$ and $0.56\% \cdot \text{min}^{-1}$ for GalNAc, Leu, and Phe, respectively. The oxidation of the Se atoms to $\text{Se}=\text{O}$ changes the hydrophilicity and allows them to come into contact with the solvent, thus, disturbing the helical structure. The breakup of helix structures can facilitate the exposure of the Se atoms to H_2O_2 to increase the reaction rate (Figure 4D). Side-chain charges, polarity, and H-bonding patterns were observed to modulate secondary structures of polypeptides; for example, the secondary structure was observed to be susceptible to the hydrophilicity of sulfone during the helix-to-coil transition as poly(L-Cys) was oxidized.⁴⁴

With a faster reaction rate, the reaction occurs readily as H_2O_2 molecules arrive at the interface. For a slower reaction, the degree of exposure of the Se atoms to H_2O_2 contributes more to the overall reaction rate. Therefore, the coupling between conformation and reaction is more pronounced with the more hydrophobic side groups. This was supported by the different curvature of the S-shaped reaction progress plot obtained from CD and NMR experiments for our sample molecules. We can only observe the reaction rate increase on the single-chain polymer of the Se-Phe sample. The cooperativity effect resembles those observed in normal polypeptides. Still, the nature of chemistry is different for coil-to-helix transition in the normal polypeptides, wherein it is more likely for hydrogen bonding to occur at the amino acid residue that already forms a hydrogen bond than that does not yet have any hydrogen bond due to the smaller entropy cost in an exothermic process.¹²

Regarding the influence of surface adsorption on the observed pathway, these polymer molecules are confined in graphene liquid pockets that are less than 100 nm thick and subjected to surface-mediated diffusion, as previously reported.²⁵ We did observe surface adsorption under our typical experimental conditions (80 kV, $3.0\text{--}6.1 \text{ e}^- \cdot \text{\AA}^2 \cdot \text{s}^{-1}$) as experiments using the same method; however, the adsorption does not seem to significantly impact the common pathway we observe, as reported for other systems.³⁹ For example, in the

event shown in Figure 3A, during the first 30 s, the intensity of the molecule showed a minor increase, likely due to the increased adsorption since stronger adsorption helps reduce the molecule motion, reflected in the higher contrast (Figure S12). After 30 s, reactions took place, causing a conformational change to follow the “head-to-tail” pathway, with the average scattering per pixel of the head quickly recovering to the same level as the tail (Figure S13).

CONCLUSIONS

In summary, we employed LP-EM methods with graphene liquid cells to directly image an intramolecular reaction of a single-chain macromolecule, resolving conformational changes as the reaction progresses. Using selenopolypeptides as a model system, we observed three transition pathways of the helix-to-coil transition: “head-to-tail,” “ends-to-center,” and “multiple coils” transition. This observation suggested that Se atoms do not have equal reaction probabilities when aligned on the polymer backbone. Quantifying the reaction kinetics, we observed cooperativity between physically constrained neighboring reaction sites and the coupling of the conformation and reaction. This cooperative effect was more pronounced in molecules with more hydrophobic side groups. Our observation highlights the critical role of coupling conformational dynamics with reaction kinetics on a single-polymer chain, offering a new perspective for polymer design, synthesis, and modification by tuning the dynamics at the single-chain level.

METHODS

Instruments

^1H NMR spectra were recorded on a 400 MHz Bruker ARX400 FT-NMR spectrometer. Size exclusion chromatography (SEC) experiments were performed on a system equipped with an isocratic pump (Model 1100, Agilent Technologies, Santa Clara, CA), a DAWN HELEOS 9-angle laser light scattering detector (MALLS, Wyatt Technology, Santa Barbara, CA), and an Optilab rEX refractive index detector (Wyatt Technology, Santa Barbara, CA). The detection wavelength of MALLS was 658 nm, and the temperature of both the refractive index and the MALLS detectors was 25 °C. Dynamic light scattering (DLS) was measured at 25 °C on a Nanobrook Omni (Brookhaven Instruments Corp., New York, USA), with a laser operating at 640 nm. Analyses were performed at an angle of 90°, collecting optics. Circular dichroism (CD) time-dependent spectra (222 nm) were recorded on a J-815 circular dichroism spectrometer J-815 (JASCO). LP-EM experiments were performed on a JEM-2100 Plus HC electron microscope with a Gatan One View IS camera. Deionized water was generated with a Milli-Q system (Merck).

Selenopolypeptide Synthesis

The synthesis of selenopolypeptide PSeO_2Na was carried out following a previously reported procedure.³⁰ The degree of polymerization (DP) of PSeO_2Na was determined to be 129 by its precursor P(pAm-SeHC) using size exclusion chromatography (SEC). According to a previous report, the modified selenopolypeptides Se-GalNAc, Se-Leu, and Se-Phe were synthesized using a postpolymerization modification process.

Ensemble Experiments

The oxidation processes of selenopolypeptides were monitored by using in situ CD and ^1H NMR spectroscopy. For in situ CD analysis, solutions of Se-GalNAc, Se-Leu, and Se-Phe (0.25–0.5 mg/mL) were prepared in phosphate-buffered saline (PBS), and one equivalent of hydrogen peroxide (H_2O_2) was added. Changes in the helicity were tracked over time by monitoring the CD signal at 222 nm. The helical content is calculated by the signal at 222 nm using the reported method,³⁴ and relative helicity is normalized by the helical content at

the initial part. For in situ ^1H NMR, Se-Leu70 and Se-Phe were dissolved in deuterium oxide (D_2O) at concentrations of 5–10 mg/mL, followed by adding one equivalent of H_2O_2 . The extent of oxidation was quantified by integrating the respective peaks, appearing at 3.75–3.90 ppm for Se-Leu70 and 3.46–3.90 ppm for Se-Phe.

Single-Molecule LP-EM Experiments

Graphene liquid cells were prepared using a modified method, as reported before.²⁵ A two-layer CVD graphene grown on copper (ACS material) was used as the bottom layer on TEM grids (microporous array carbon film, R1.2/1.3 on 300 mesh gold grids purchased from Beijing EBO Tech. Ltd.). Three to five layers of CVD graphene grown on copper (ACS material) were etched in 0.1 M ammonium persulfate (Sigma-Aldrich) solution and then transferred by glass plate into deionized water, followed by heating at 37 °C for 2 h to remove the remaining ammonium persulfate. Sample solutions were prepared according to the conditions in Table S1. Samples were loaded onto a JEM-2100 Plus HC electron microscope with a Gatan One View IS camera. Imaging conditions are also listed in Table S1. The capture interval (and the frame rate, with no i/o lagging) is set to 0.1594 s per frame to capture the conformational change as quickly as possible while maintaining a sufficient signal-to-noise ratio for quantitative analysis.

LP-EM Data Analysis

LP-EM raw data dm4 files were converted into dm3 files with the Gatan Microscopy Suite for analysis in ImageJ. Drift correction was performed with the “template-matching” plugin in ImageJ. Every three images after drift correction were rolling averaged for better contrast. Regions of interest were extracted and shown in the main text figure or used to generate binary masks by UNet++⁴⁰ after brightness/contrast adjustment. Unadjusted images were used for the quantitative analysis of electron scattering. Wrongly marked or incomplete binary masks were manually corrected. From the binarized images, size and shape changes can be quantified using customized written codes.

Average background electron transmission I_b is the average intensity of all pixels of a selected region as close as possible to the molecule of interest. Electron scattering by the molecule I_s was calculated using the total intensity of masked region I_{ROI} minus the background electron transmission (pixel counts $\times I_b$). The thickness of the molecule is less than 10 nm; therefore, we consider a linear relationship between I_s and the actual molecular mass, and we can use I_s to represent the mass of molecules. The average scattering per pixel $I_{s,\text{ave}}$ was calculated by I_s/pixel counts of the masked region, reflecting the molecule's average thickness or compactness of conformation. The LP-EM figures shown in the main text are adjusted by brightness and contrast for a better visual effect. All of the calculations are accomplished by Python scripts using unadjusted data.

■ ASSOCIATED CONTENT

SI Supporting Information

The Supporting Information is available free of charge at <https://pubs.acs.org/doi/10.1021/jacsau.4c00928>.

Sample preparation details and characterization, TEM parameter setups, detailed TEM image analysis of Se-GalNac, Se-Leu, and Se-Phe, time-resolved NMR spectra of Se-Phe and Se-Leu70 oxidized by 1 eq H_2O_2 (Table S1 and Figures S1–S13) (PDF)

In situ LP-EM movie of Se-GalNac showing direct degradation under 200 kV (AVI)

In situ LP-EM movie of reversibly absorbed Se-Leu (AVI)

In situ LP-EM movie of the head-to-tail pathway in Se-GalNac (AVI)

In situ LP-EM movie of the ends-to-center pathway in Se-GalNac (AVI)

In situ LP-EM movie of the multiple coils pathway in Se-GalNac (AVI)

In situ LP-EM movie of the head-to-tail pathway in Se-Phe (AVI)

In situ LP-EM movie of the ends-to-center pathway in Se-Leu (AVI)

■ AUTHOR INFORMATION

Corresponding Authors

Hua Lu – Beijing National Laboratory for Molecular Sciences, College of Chemistry and Molecular Engineering, Key Laboratory of Polymer Chemistry & Physics, Beijing 100871, People's Republic of China; orcid.org/0000-0003-2180-3091; Email: chemhualu@pku.edu.cn

Huan Wang – Beijing National Laboratory for Molecular Sciences, College of Chemistry and Molecular Engineering, Key Laboratory of Polymer Chemistry & Physics, Beijing 100871, People's Republic of China; National Biomedical Imaging Center, Peking University, Beijing 100871, People's Republic of China; orcid.org/0000-0002-2542-936X; Email: wanghuan_ccme@pku.edu.cn

Authors

Zuo Zhang – Beijing National Laboratory for Molecular Sciences, College of Chemistry and Molecular Engineering, Key Laboratory of Polymer Chemistry & Physics, Beijing 100871, People's Republic of China

Haisen Zhou – Beijing National Laboratory for Molecular Sciences, College of Chemistry and Molecular Engineering, Key Laboratory of Polymer Chemistry & Physics, Beijing 100871, People's Republic of China

Zhun Xu – Beijing National Laboratory for Molecular Sciences, College of Chemistry and Molecular Engineering, Key Laboratory of Polymer Chemistry & Physics, Beijing 100871, People's Republic of China

Guangqi Wu – Beijing National Laboratory for Molecular Sciences, College of Chemistry and Molecular Engineering, Key Laboratory of Polymer Chemistry & Physics, Beijing 100871, People's Republic of China; Present Address: Department of Chemistry, Oxford University, Oxford, OX1 2JD, United Kingdom; orcid.org/0000-0002-9763-6982

Complete contact information is available at: <https://pubs.acs.org/10.1021/jacsau.4c00928>

Author Contributions

||Z.Z. and H.Z. contributed equally. H.W. and H.L. initiated the experiments, and Z.Z., H.Z., Z.X. and G.W. performed the experiments. The manuscript was written through the contributions of all authors. All authors have given approval to the final version of the manuscript.

Funding

The work is mainly supported by the Natural Science Foundation of China (22174006 to HW and 22125101, 22331002 to HL) and the Beijing National Laboratory for Molecular Sciences (BNLMS-CXXM-202008).

Notes

The authors declare no competing financial interest.

■ ACKNOWLEDGMENTS

We thank the NMR Center and Center for Instrumental Analysis at Peking University for their kind assistance.

■ ABBREVIATIONS

PN-g-PBLG, polynorbornene-g-poly(γ -benzyl-L-glutamate); ROMP, ring-opening metathesis polymerization; T-jump, laser-induced temperature-jump; CD, circular dichroism; NMR, nuclear magnetic resonance spectroscopy; LP-EM, liquid-phase electron microscopy; Sec, selenocysteines; DP, degree of polymerization; H₂O₂, hydrogen peroxide; D₂O, deuterium oxide

■ REFERENCES

- (1) Widom, B. Collision theory of chemical reaction rates. *Adv. Chem. Phys.* **1963**, *5*, 353–386.
- (2) Laidler, K. J.; King, M. C. Development of transition-state theory. *J. Phys. Chem.* **1983**, *87* (15), 2657–2664.
- (3) Baumgartner, R.; Fu, H.; Song, Z.; Lin, Y.; Cheng, J. Cooperative polymerization of α -helices induced by macromolecular architecture. *Nat. Chem.* **2017**, *9* (7), 614–622.
- (4) Easter, Q. T.; Blum, S. A. Kinetics of the same reaction monitored over nine orders of magnitude in concentration: When are unique subensemble and single-turnover reactivity displayed? *Angew. Chem., Int. Ed.* **2018**, *57* (37), 12027–12032.
- (5) Ye, R.; Sun, X.; Mao, X.; Alfonso, F. S.; Baral, S.; Liu, C.; Coates, G. W.; Chen, P. Optical sequencing of single synthetic polymers. *Nat. Chem.* **2024**, *16* (2), 210–217.
- (6) Liu, C.; Kubo, K.; Wang, E.; Han, K.-S.; Yang, F.; Chen, G.; Escobedo, F. A.; Coates, G. W.; Chen, P. Single polymer growth dynamics. *Science* **2017**, *358* (6361), 352–355.
- (7) Wang, H.; Park, M.; Dong, R.; Kim, J.; Cho, Y.-K.; Tlustý, T.; Granick, S. Boosted molecular mobility during common chemical reactions. *Science* **2020**, *369* (6503), 537–541.
- (8) Wang, D.; Frechette, L. B.; Best, R. B. On the role of native contact cooperativity in protein folding. *Proc. Natl. Acad. Sci. U. S. A.* **2024**, *121* (22), No. e2319249121.
- (9) Dai, S.; Funk, L.-M.; von Pappenheim, F. R.; Sautner, V.; Paulikat, M.; Schröder, B.; Uranga, J.; Mata, R. A.; Tittmann, K. Low-barrier hydrogen bonds in enzyme cooperativity. *Nature* **2019**, *573* (7775), 609–613.
- (10) Ganguly, A.; Rajdev, P.; Williams, S. M.; Chatterji, D. Nonspecific interaction between DNA and protein allows for cooperativity: A case study with mycobacterium DNA binding protein. *J. Phys. Chem. B* **2012**, *116* (1), 621–632.
- (11) Lu, H. P.; Xun, L.; Xie, X. S. Single-molecule enzymatic dynamics. *Science* **1998**, *282* (5395), 1877–1882.
- (12) Huang, C.-Y.; Getahun, Z.; Zhu, Y.; Klemke, J. W.; DeGrado, W. F.; Gai, F. Helix formation via conformation diffusion search. *Proc. Natl. Acad. Sci. U. S. A.* **2002**, *99* (5), 2788–2793.
- (13) Williams, S.; Causgrove, T. P.; Gilmanshin, R.; Fang, K. S.; Callender, R. H.; Woodruff, W. H.; Dyer, R. B. Fast events in protein folding: Helix melting and formation in a small peptide. *Biochemistry* **1996**, *35* (3), 691–697.
- (14) Clarke, D. T.; Doig, A. J.; Stapley, B. J.; Jones, G. R. The α -helix folds on the millisecond time scale. *Proc. Natl. Acad. Sci. U. S. A.* **1999**, *96* (13), 7232–7237.
- (15) Thompson, P. A.; Muñoz, V.; Jas, G. S.; Henry, E. R.; Eaton, W. A.; Hofrichter, J. The helix-coil kinetics of a heteropeptide. *J. Phys. Chem. B* **2000**, *104* (2), 378–389.
- (16) Lednev, I. K.; Karnoup, A. S.; Sparrow, M. C.; Asher, S. A. Transient UV Raman spectroscopy finds no crossing barrier between the peptide α -helix and fully random coil conformation. *J. Am. Chem. Soc.* **2001**, *123* (10), 2388–2392.
- (17) Nesmelova, I.; Krushelnitsky, A.; Idiyatullin, D.; Blanco, F.; Ramirez-Alvarado, M.; Daragan, V. A.; Serrano, L.; Mayo, K. H. Conformational exchange on the microsecond time scale in α -helix and β -hairpin peptides measured by ¹³C NMR transverse relaxation. *Biochemistry* **2001**, *40* (9), 2844–2853.
- (18) Bryngelson, J. D.; Onuchic, J. N.; Socci, N. D.; Wolynes, P. G. Funnels, pathways, and the energy landscape of protein folding: A synthesis. *Proteins: Struct., Funct., Bioinf.* **1995**, *21* (3), 167–195.
- (19) Wang, J.; Lu, H.; Ren, Y.; Zhang, Y.; Morton, M.; Cheng, J.; Lin, Y. Interrupted helical structure of grafted polypeptides in brush-like macromolecules. *Macromolecules* **2011**, *44* (22), 8699–8708.
- (20) Ren, Y.; Fu, H.; Baumgartner, R.; Zhang, Y.; Cheng, J.; Lin, Y. Folding cooperativity of synthetic polypeptides with or without “tertiary” interactions. *ACS Macro Lett.* **2017**, *6* (7), 733–737.
- (21) Wang, W.; Fu, H.; Lin, Y.; Cheng, J.; Song, Z. Cooperative covalent polymerization of N-carboxyanhydrides: from kinetic studies to efficient synthesis of polypeptide materials. *Acc. Mater. Res.* **2023**, *4* (7), 604–615.
- (22) Scott, W. A.; Gharakhanian, E. G.; Bell, A. G.; Evans, D.; Barun, E.; Houk, K. N.; Deming, T. J. Active controlled and tunable coacervation using side-chain functional α -helical homopolypeptides. *J. Am. Chem. Soc.* **2021**, *143* (43), 18196–18203.
- (23) Nagamanasa, K. H.; Wang, H.; Granick, S. Liquid-cell electron microscopy of adsorbed polymers. *Adv. Mater.* **2017**, *29* (41), 1703555.
- (24) Wang, H.; Li, B.; Kim, Y. J.; Kwon, O. H.; Granick, S. Intermediate states of molecular self-assembly from liquid-cell electron microscopy. *Proc. Natl. Acad. Sci. U. S. A.* **2020**, *117* (3), 1283–1292.
- (25) Wang, H.; Xu, Z.; Mao, S.; Granick, S. Experimental guidelines to image transient single-molecule events using graphene liquid cell electron microscopy. *ACS Nano* **2022**, *16* (11), 18526–18537.
- (26) Smith, J. W.; Carnevale, L. N.; Das, A.; Chen, Q. Electron videography of a lipid–protein tango. *Sci. Adv.* **2024**, *10* (16), No. eadk0217.
- (27) Park, J.; Jeong, H.; Noh, N.; Park, J. S.; Ji, S.; Kang, S.; Huh, Y.; Hyun, J.; Yuk, J. M. Single-molecule graphene liquid cell electron microscopy for instability of intermediate amyloid fibrils. *Adv. Mater.* **2024**, *36* (6), No. e2309936.
- (28) Yuan, Y.; Dong, X.; Wang, H.; Gai, F. Capturing the illusive ring-shaped intermediates in A β 42 amyloid formation. *Biophys. Rev.* **2024**, *5* (3), 032104.
- (29) Wu, G.; Ge, C.; Liu, X.; Wang, S.; Wang, L.; Yin, L.; Lu, H. Synthesis of water soluble and multi-responsive selenopolypeptides via ring-opening polymerization of N-carboxyanhydrides. *Chem. Commun.* **2019**, *55* (54), 7860–7863.
- (30) Wu, G.; Zhou, H.; Zhang, J.; Tian, Z.-Y.; Liu, X.; Wang, S.; Coley, C. W.; Lu, H. A high-throughput platform for efficient exploration of functional polypeptide chemical space. *Nat. Synth.* **2023**, *2* (6), 515–526.
- (31) Woznichak, M. M.; Overcast, J. D.; Robertson, K.; Neumann, H. M.; May, S. W. Reaction of phenylaminoethyl selenides with peroxynitrite and hydrogen peroxide. *Arch. Biochem. Biophys.* **2000**, *379* (2), 314–320.
- (32) Ribaldo, G.; Bellanda, M.; Menegazzo, I.; Wolters, L. P.; Bortoli, M.; Ferrer-Sueta, G.; Zagotto, G.; Orian, L. Mechanistic insight into the oxidation of organic phenylselenides by H₂O₂. *Chem.–Eur. J.* **2017**, *23* (10), 2405–2422.
- (33) Reeves, M. A.; Hoffmann, P. R. The human selenoproteome: recent insights into functions and regulation. *Cell. Mol. Life Sci.* **2009**, *66* (15), 2457–2478.
- (34) McLean, L. R.; Hagaman, K. A.; Owen, T. J.; Krstenansky, J. L. Minimal peptide length for interaction of amphipathic α -helical peptides with phosphatidylcholine liposomes. *Biochemistry* **1991**, *30* (1), 31–37.
- (35) Schellman, J. A. The factors affecting the stability of hydrogen-bonded polypeptide structures in solution. *J. Phys. Chem.* **1958**, *62* (12), 1485–1494.
- (36) Schneider, N. M.; Norton, M. M.; Mendel, B. J.; Grogan, J. M.; Ross, F. M.; Bau, H. H. Electron–water interactions and implications for liquid cell electron microscopy. *J. Phys. Chem. C* **2014**, *118* (38), 22373–22382.

(37) Wilcox, K. G.; Dingle, M. E.; Saha, A.; Hore, M. J. A.; Morozova, S. Persistence length of alpha-helical poly-L-lysine. *Soft Matter* **2022**, *18* (35), 6550–6560.

(38) Touve, M. A.; Figg, C. A.; Wright, D. B.; Park, C.; Cantlon, J.; Sumerlin, B. S.; Gianneschi, N. C. Polymerization-induced self-assembly of micelles observed by liquid cell transmission electron microscopy. *ACS Cent. Sci.* **2018**, *4* (5), 543–547.

(39) Li, J.-Y.; Liu, F.; Xu, J.; Kim, Y.-J.; Kwon, O.-H.; Xia, B.; Wang, H.; Granick, S. The ergodicity question when imaging DNA conformation using liquid cell electron microscopy. *Proc. Natl. Acad. Sci. U. S. A.* **2024**, *121* (3), No. e2314797121.

(40) Cheng, B.; Ye, E.; Sun, H.; Wang, H. Deep learning-assisted analysis of single molecule dynamics from liquid-phase electron microscopy. *Chem. Commun.* **2023**, *59* (12), 1701–1704.

(41) Zimm, B. H.; Bragg, J. K. Theory of the phase transition between helix and random coil in polypeptide chains. *J. Chem. Phys.* **1959**, *31* (2), 526–535.

(42) Zimm, B. H.; Doty, P.; Iso, K. Determination of the parameters for helix formation in poly- γ -benzyl-glutamate. *Proc. Natl. Acad. Sci. U. S. A.* **1959**, *45* (11), 1601–1607.

(43) Ren, Y.; Baumgartner, R.; Fu, H.; van der Schoot, P.; Cheng, J.; Lin, Y. Revisiting the helical cooperativity of synthetic polypeptides in solution. *Biomacromolecules* **2017**, *18* (8), 2324–2332.

(44) Kramer, J. R.; Deming, T. J. Multimodal switching of conformation and solubility in homocysteine derived polypeptides. *J. Am. Chem. Soc.* **2014**, *136* (15), 5547–5550.